frontiers | Frontiers in Marine Science

TYPE Original Research
PUBLISHED 06 October 2022
DOI 10.3389/fmars.2022.1034945

OPEN ACCESS

EDITED BY
Weihua Jiao,
Shanghai Jiao Tong University, China

REVIEWED BY
Cheng-shi Jiang,
University of Jinan, China
Hui Cui,
Guangzhou University of Chinese Medicine, China

*CORRESPONDENCE
Ling Liu
liul@im.ac.cn

†These authors have contributed equally to this work

SPECIALTY SECTION
This article was submitted to Marine Biotechnology and Bioproducts, a section of the journal Frontiers in Marine Science

RECEIVED 02 September 2022
ACCEPTED 22 September 2022
PUBLISHED 06 October 2022

CITATION
Zhang R, Zhang J, Huo R, Xue Y, Hong K and Liu L (2022) Sulfur-containing benzofurans and α-pyrones from the mangrove-derived fungus *Talaromyces* sp. WHUF0341. *Front. Mar. Sci.* 9:1034945. doi: 10.3389/fmars.2022.1034945

Sulfur-containing benzofurans and α-pyrones from the mangrove-derived fungus *Talaromyces* sp. WHUF0341

Ruohan Zhang[1,2†], Jinxin Zhang[1,2†], Ruiyun Huo[1,2], Yaxin Xue[3], Kui Hong[3] and Ling Liu[1,2*]

[1]State Key Laboratory of Mycology, Institute of Microbiology, Chinese Academy of Sciences, Beijing, China, [2]Department of Radiation and Medical Oncology, Zhongnan Hospital, Key Laboratory of Combinatorial Biosynthesis and Drug Discovery, Ministry of Education, School of Pharmaceutical Sciences, Wuhan University, Wuhan, China, [3]College of Life Sciences, University of Chinese Academy of Sciences, Beijing, China

Two new sulfur-containing benzofurans, talarobenzofurans A and B (**1** and **2**), one new benzofuran talarobenzofuran C (**3**) and two new α-pyrones talaropyrones A and B (**5** and **6**), along with five known compounds eurothiocin A (**4**), nodulisporipyrone A (**7**), peniazaphilin B (**8**), ramulosin (**9**) and 6-hydroxyramulosin (**10**) were isolated and identified from the culture extract of the mangrove-derived fungus *Talaromyces* sp. WHUF0341 guided by OSMAC (one strain-many compounds) strategy. Their structures were established by extensive spectroscopic data analysis, the modified Mosher's method and electronic circular dichroism (ECD) calculations. Structurally, compounds **1** and **2** possessed the unique thioester moiety derived from benzofuran and 2-hydroxy-3-mercaptopropionic acid, which was rarely-observed in natural products. The α-glucosidase inhibitory and antibacterial activities of the isolated compounds were evaluated. Compounds **3** and **4** exhibited inhibitory effects against α-glucosidase activity with IC_{50} values of 48.9 $\pm$ 2.16 and 8.8 $\pm$ 1.08 μM, respectively. The inhibitory type of **3** on α-glucosidase was determined as non-competitive-type inhibition with K_i value of 242.3 μM by using Lineweaver-Burk double reciprocal and Dixon single reciprocal plots. Meanwhile, the binding model of **3** and **4** with α-glucosidase was determined by molecular docking assay. The biosynthetic pathways of compounds **1**–**4** were also proposed. This study suggested that benzofurans **3** and **4** could be potential lead compounds for the hypoglycemic drugs.

KEYWORDS

***Talaromyces* sp., mangrove-derived fungus, thioester, α-glucosidase inhibitory activity, sulfur-containing benzofurans, molecular docking**

Introduction

Fungi are considered to be rich sources of biologically active compounds for drug discovery (Newman and Cragg, 2020; Carroll et al., 2021). However, due to the rediscovery of previously described natural products of fungi from traditionally investigated habitats, the attention of researchers has been increasingly attracted to fungi from unique ecological niches such as mangrove-derived fungi (El-Bondkly et al., 2021). Mangroves are a diverse group of higher plants vegetating in the intertidal zones in subtropical and tropical climates (Ellison and Farnsworth, 1992; Nagelkerken et al., 2008). Mangrove-derived fungi, living in these unique environments, are considered as a new resource for diverse secondary metabolites with a wide range of bioactivities, including cytotoxic (Meng et al., 2016; Liu et al., 2021a; Tao et al., 2021), antimicrobial (Hemberger et al., 2013; Valente et al., 2020), enzyme inhibitory (Liu et al., 2014), anti-inflammatory (Liu et al., 2018), antioxidative (Guo et al., 2015) and antiviral activities (Yu et al., 2016).

As a part of our ongoing search for novel bioactive metabolites from mangrove-derived fungi (Liu et al., 2021b; Hou et al., 2021), the strain *Talaromyces* sp. WHUF0341, isolated from a sample of mangrove soil in Yalong Bay, Hainan Province, People's Republic of China, was screened out for a detailed chemical investigation. To expand the chemical diversity of secondary metabolites, this strain was cultured in different media (Supplementary Table S1) using the OSMAC (one strain-many compounds) strategy (Pan et al., 2019). HPLC-UV analysis (Supplementary Figure S1) showed that the secondary metabolites in solid rice medium with 3% sea salt are more abundant than those in other culture media. Large scale fermentation on this medium was then performed for 30 days. Chemical investigation of the EtOAc extract of this fungus led to the isolation of five new compounds, talarobenzofurans A–C (**1**–**3**) and talaropyrones A and B (**5** and **6**), along with five known compounds eurothiocin A (**4**) (Liu et al., 2014), nodulisporipyrone A (**7**) (Zhao et al., 2015), peniazaphilin B (**8**) (Zhang et al., 2018), ramulosin (**9**) (Wang et al., 2014) and 6-hydroxyramulosin (**10**) (McMullin et al., 2017) (Figure 1). All of the isolated compounds were evaluated for their α-glucosidase inhibitory and antibacterial activities. Herein, we report the isolation, structure elucidation, bioactivities and putative biosynthetic pathways of these compounds.

Materials and methods

General experimental procedures

The ECD spectra were measured on a Chirascan V100 instrument (Applied Photophysics Ltd, Leatherhead, Surrey, UK). Optical rotations were measured with an Anton Paar MCP 200 Automatic Polarimeter (Anton Paar, Graz, Austria). UV data were recorded using a Thermo Genesys-10S UV/Vis spectrophotometer (Thermo Fisher Scientific, Waltham, MA, USA). IR data were obtained on a Nicolet IS5 FT-IR spectrophotometer (Thermo Fisher Scientific, Waltham, MA, USA). ^{1}H and ^{13}C NMR data were acquired with Bruker Avance-500 spectrometer (Bruker, Bremen, Germany) using solvent signals (Acetone-d_6: $\delta_{C/H}$ 29.8, 206.1/2.05; $CDCl_3$: $\delta_{C/H}$ 77.2/7.26; DMSO-d_6: $\delta_{C/H}$ 39.5/2.50) as references. Mass data were performed on an Agilent Accurate-Mass-Q-TOF LC/MS 6520 instrument (Agilent Technologies, Santa Clara, CA, USA). HPLC separations were performed on an Agilent 1260 instrument equipped with a variable-wavelength UV detector with a flow rate of 2.0 mL/min. α-Glucosidase (from *Saccharomyces cerevisiae*, 33 U/mg), *p*-nitrophenyl-α-D-glucopyranoside (*p*-NPG) and acarbose purchased from Shanghai yuanye Bio-Technology Co., Ltd (Shanghai, China).

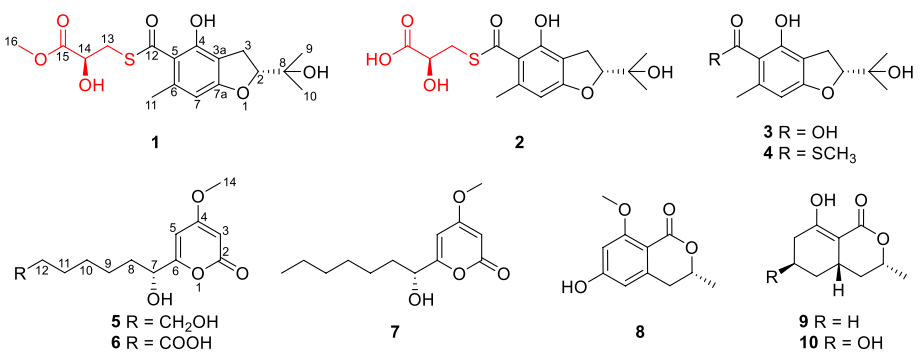

FIGURE 1
Structures of compounds 1–10.

Fungal material

The sample of mangrove soil was collected from the Yalong Bay, Hainan Province, People's Republic of China. The fungal strain WHUF0341 was isolated on MEA medium (1.5% sea salt, 1.7% malt extract, 0.3% peptone, 0.2% agar) from this sample and preserved in sterilized 30% glycerol at -80°C. Phylogenetic analysis based on ITS sequence and morphological observation indicated that the strain WHUF0341 should be identified as *Talaromyces* sp. (GenBank Accession No. ON564542.1). The strain was deposited in the Institute of Microbiology, Chinese Academy of Sciences, Beijing.

Fermentation

Four liquid media and two solid media (each medium contained 3% sea salt as control) were tested to identify the optimum culture conditions (Supplementary Table S1). The fungus *Talaromyces* sp. WHUF0341 was grown on potato dextrose agar (PDA) at 28°C for 10 days. Several pieces of agar plugs (about 0.5 × 0.5 × 0.5 cm^3) were then inoculated into 250 mL Erlenmeyer flasks containing 50 mL of media (0.4% glucose, 1% malt extract, and 0.4% yeast extract) at room temperature on an orbital shaker at 200 rpm for 3 days to produce the seed culture. Finally, 5.0 mL of the spore inoculums obtained from liquid phase cultivation was transferred into 50 × 500 mL Erlenmeyer flasks each containing 80 g rice medium and 120 mL of distilled H_2O with 3% sea salt and incubated at 25°C under static condition for 30 days.

Extraction and isolation

The fermented rice material was extracted repeatedly with EtOAc for three times, and the combined filtrate was evaporated to dryness under reduced pressure to afford the crude extract (65.0 g). The crude extract was then fractionated by silica gel vacuum liquid chromatography (VLC) eluted with a gradient of petroleum ether (PE)/EtOAc (from 20:1 to 1:2, v/v) to get seven fractions (Fr. 1–7). The fraction 2 (0.6 g, eluted with PE/EtOAc 4:1) was fractionated by Sephadex LH-20 column chromatography (CC) eluting with CH_2Cl_2/MeOH 1:1 to afford compounds **4** (7.0 mg) and **9** (6.3 mg). The fraction 3 (5.4 g, eluted with PE/EtOAc 1:1) was subjected to octadecylsilyl column chromatography (ODS CC) with MeOH-H_2O gradient elution to yield nine subfractions (Fr. 3-1–3-9). The subfraction 3-2 (49.0 mg, eluted with 60% MeOH-H_2O) was purified by semi-preparative RP-HPLC (Agilent Zorbax SB-C18 column; 5 μm; 10 × 250 mm; 34% CH_3CN-H_2O for 35 min; 2.0 mL/min) to afford compound **1** (5.0 mg, t_R 23.2 min). The subfraction 3-5 (44.0 mg, eluted with 65% MeOH-H_2O) was further purified by semi-preparative RP-HPLC (40% CH_3CN-H_2O for 50 min; 2.0 mL/min) to obtain compound **7** (7.3 mg, t_R 43.5 min). The fraction 4 (1.4 g, eluted with PE/EtOAc 1:2) was subjected to ODS CC using a MeOH-H_2O gradient elution and the subfraction 4-2 (93.0 mg, eluted with 30% MeOH-H_2O) was further purified by semi-preparative RP-HPLC (30% CH_3CN-H_2O for 15 min; 2.0 mL/min) to get compound **8** (6.1 mg, t_R 11.6 min). The subfraction 4-4 (52.0 mg, eluted with 40% MeOH-H_2O) was also purified by semi-preparative RP-HPLC (50% MeOH-H_2O for 25 min; 2.0 mL/min) to afford compound **6** (2.3 mg, t_R 13.0 min). The fraction 5 (0.6 g, eluted with PE/EtOAc 3:7) was refractionated by Sephadex LH-20 CC eluting with MeOH and the subfraction 5-1 (102.0 mg) was purified by semi-preparative RP-HPLC (55% MeOH-H_2O for 50 min; 2.0 mL/min) to obtain compound **2** (4.8 mg, t_R 41.2 min). The fraction 6 (2.9 g, eluted with PE/EtOAc 1:3) was chromatographed on an ODS column using a gradient eluent of MeOH-H_2O, the fraction 6-4 (63.0 mg, eluted with 30% MeOH-H_2O) was purified by semi-preparative RP-HPLC (28% CH_3CN-H_2O for 40 min; 2.0 mL/min) to yield compounds **3** (2.2 mg, t_R 29.2 min) and **5** (1.4 mg, t_R 13.6 min). The fraction 7 (0.2 g, eluted with PE/EtOAc 1:9) was separated by Sephadex LH-20 CC eluting with MeOH to yield three fractions (Fr. 7-1–7-3), the fraction 7-2 (15.3 mg) was purified by semi-preparative RP-HPLC (25% CH_3CN-H_2O for 22 min; 2.0 mL/min) to afford compound **10** (2.0 mg, t_R 15.0 min).

Talarobenzofuran A (***1***): yellow oil; $[\alpha]_D^{25}$ −58.9 (*c* 0.1, MeOH); UV (MeOH) λ_{max} (log ϵ) 229 (2.12), 275 (2.01) nm; ECD (*c* 0.54 × 10^{-3} M, MeOH) λ_{max} ($\Delta\epsilon$) 219 (−1.03), 242 (−0.22), 272 (−1.73), 329 (+0.10) nm; IR (neat) ν_{max} 3420, 2973, 1743, 1635, 1277, 1233, 1148 cm^{-1}; ^1H and ^{13}C NMR data, see Table 1; HRESIMS *m/z* 371.1168 $[M + H]^+$ (calcd for $C_{17}H_{23}O_7S$, 371.1159).

Talarobenzofuran B (***2***): yellow oil; $[\alpha]_D^{25}$ −60.9 (*c* 0.1, MeOH); UV (MeOH) λ_{max} (log ϵ) 229 (2.13), 271 (1.93) nm; ECD (*c* 0.77 × 10^{-3} M, MeOH) λ_{max} ($\Delta\epsilon$) 215 (−1.33), 239 (+0.03), 276 (−1.24), 344 (−0.01) nm; IR (neat) ν_{max} 3367, 2975, 1721, 1636, 1233, 1023 cm^{-1}; ^1H and ^{13}C NMR data, see Table 1; HRESIMS *m/z* 357.1010 $[M + H]^+$ (calcd for $C_{16}H_{21}O_7S$, 357.1003).

Talarobenzofuran C (***3***): yellow oil; $[\alpha]_D^{25}$−49.9 (*c* 0.1, MeOH); UV (MeOH) λ_{max} (log ϵ) 229 (2.15), 267 (1.99) nm; ECD (*c* 0.79 × 10^{-3} M, MeOH) λ_{max} ($\Delta\epsilon$) 211 (−2.13), 230 (−0.20), 266 (−2.06), 332 (+0.01) nm; IR (neat) ν_{max} 3420, 2974, 1616, 1358, 1270, 1161, 1089 cm^{-1}; ^1H and ^{13}C NMR data, see Table 1; HRESIMS *m/z* 253.1077 $[M + H]^+$ (calcd for $C_{13}H_{17}O_5$, 253.1071).

Talaropyrone A (***5***): white solid; $[\alpha]_D^{25}$+65.9 (*c* 0.1, MeOH); UV (MeOH) λ_{max} (log ϵ) 207 (2.20), 280 (2.05) nm; ECD (*c* 0.78 × 10^{-3} M, MeOH) λ_{max} ($\Delta\epsilon$) 205 (−7.66), 282 (+4.60), 320 (+0.20) nm; IR (neat) ν_{max} 3391, 2931, 1694, 1567, 1456, 1246 cm^{-1}; ^1H and ^{13}C NMR data, see Table 2; HRESIMS *m/z* 279.1206 $[M + Na]^+$ (calcd for $C_{13}H_{20}O_5Na$, 279.1203).

Talaropyrone B (***6***): light yellow solid; $[\alpha]_D^{25}$ +67.0 (*c* 0.1, MeOH); UV (MeOH) λ_{max} (log ϵ) 210 (2.02), 280 (2.05) nm; ECD (*c* 0.74 × 10^{-3} M, MeOH) λ_{max} ($\Delta\epsilon$) 205 (−1.62), 282

10.3389/fmars.2022.1034945

TABLE 1 NMR data for compounds 1–3 (δ in ppm, J in Hz).

Pos.	1[a]		2[a]		3[b]	
	δ_H (J in Hz)	δ_C	δ_H (J in Hz)	δ_C	δ_H (J in Hz)	δ_C
2	4.69, dd (9.5, 8.0)	91.8, CH	4.70, dd (9.5, 8.0)	91.8, CH	4.73, dd (9.5, 8.0)	91.5, CH
3	3.14, dd (15.5, 8.0) 3.08, dd (15.5, 9.5)	28.3, CH_2	3.14, dd (15.5, 8.0) 3.08, dd (15.5, 9.5)	28.3, CH_2	3.14, dd (16.0, 9.5) 3.06, dd (16.0, 8.0)	27.7, CH_2
3a		112.5, C		112.5, C		111.3, C
4		155.1, C		155.0, C		161.2, C
5		119.5, C		110.9, C		104.5, C
6		139.7, C		139.8, C		145.8, C
7	6.22, s	105.3, CH	6.22, s	105.3, CH	6.29, s	106.0, CH
7a		164.9, C		164.9, C		165.7, C
8		71.6, C		71.5, C		72.2, C
9	1.20, s	26.2, CH_3	1.21, s	26.1, CH_3	1.34, s	26.0, CH_3
10	1.24, s	25.6, CH_3	1.25, s	25.6, CH_3	1.22, s	23.9, CH_3
11	2.41, s	22.3, CH_3	2.43, s	22.4, CH_3	2.56, s	24.9, CH_3
12		195.7, C		195.8, C		175.5, C
13	3.52, dd (13.5, 4.5) 3.37, dd (13.5, 6.5)	34.6, CH_2	3.61, dd (13.5, 4.5) 3.36, dd (13.5, 7.0)	34.7, CH_2		
14	4.43, ddd (13.0, 6.5, 1.5)	70.6, CH	4.43, dd (5.0, 4.5)	70.2, CH		
15		173.6, C		174.1, C		
16	3.73, s	52.6, CH_3				
4-OH	9.79, s				11.56, brs	
8-OH	3.70, br s					
13-OH	4.76, d (6.5)					

[a]Recorded in acetone-d_6.
[b]Recorded in $CDCl_3$.

TABLE 2 NMR data for compounds 5 and 6 (δ in ppm, J in Hz).

Pos.	5[a]		6[b]	
	δ_H (J in Hz)	δ_C, mult.	δ_H (J in Hz)	δ_C, mult.
2		163.3, C		164.0, C
3	5.54, d (2.0)	87.6, CH	5.42, d (2.5)	88.3, CH
4		171.0, C		172.1, C
5	6.11, d (2.0)	97.8, CH	6.12, dd (2.5, 1.0)	98.5, CH
6		167.8, C		168.8, C
7	4.23, dt (8.0, 5.0)	68.9, CH	4.37, dd (8.0, 4.5)	70.9, CH
8	1.64, m 1.53, m	34.6, CH_2	1.66, m 1.80, m	35.9, CH_2
9	1.31, m	24.6, CH_2	1.47, m	25.6, CH_2
10	1.26, m	28.7, CH_2	1.39, m	29.7, CH_2
11	1.26, m	25.4, CH_2	1.61, m	25.6, CH_2
12	1.39, m	32.4, CH_2	2.29, t (7.5)	34.2, CH_2
13	3.36, m	60.7, CH_2		174.7, C
14	3.81, s	56.3, CH_3	3.87, s	56.7, CH_3
7-OH	5.59, d (5.5)			
13-OH	4.32, t (5.0)			

[a]Recorded in DMSO-d_6.
[b]Recorded in acetone-d_6.

(+0.91), 317 (+0.04) nm; IR (neat) ν_{max} 3350, 2940, 1694, 1627, 1564, 1257 cm^{-1}; ^{1}H and ^{13}C NMR data, see Table 2; HRESIMS *m/z* 293.1001 $[M + Na]^+$ (calcd for $C_{13}H_{18}O_6Na$, 293.0996).

Preparation of (*R*)-MTPA ester (1a) and (*S*)-MTPA ester (1b)

Compound **1** (0.5 mg for each) was dissolved in pyridine-d_5 (100 μL) and transferred into clean NMR tubes, then *S*-MTPA chloride (10 μL) and *R*-MTPA chloride (10 μL) were added to each of the NMR tubes, and reaction mixture was stirred at room temperature overnight, which afforded the (*R*)-MTPA ester and (*S*)-MTPA ester derivatives of compound **1**. ^{1}H NMR data were obtained directly from the reaction NMR tubes. The $\Delta\delta_H = \delta_{H(S)\text{-MTPA-ester}} - \delta_{H(R)\text{-MTPA-ester}}$ values around the stereogenic centers of the MTPA esters were determined by ^{1}H NMR spectra.

(R)-MTPA ester of ***1*** *(**1a**)*: ^{1}H NMR (pyridine-d_5, 500 MHz) δ_H 6.574 (1H, d, *J* = 14.8 Hz, H-7), 4.867 (1H, m, H-2), 3.841 (3H, m, H-16), 3.533 (2H, m, H-13), 3.308 (2H, s, H-3), 2.245 (3H, m, H-11), 1.504 (3H, s, H-10), 1.386 (3H, s, H-9).

(S)-MTPA ester of ***1*** *(**1b**)*: ^{1}H NMR (pyridine-d_5, 500 MHz) δ_H 6.587 (1H, d, *J* = 16.9 Hz, H-7), 4.920 (1H, m, H-2), 3.838 (3H, br s, H-16), 3.538 (2H, d, *J* = 9.7 Hz, H-13), 3.306 (2H, br s, H-3), 2.256 (3H, m, H-11), 1.480 (3H, d, *J* = 3.9 Hz, H-10), 1.379 (3H, d, *J* = 5.9 Hz, H-9).

ECD calculation methods

Conformational analysis within an energy window of 3.0 kcal/mol was performed by using the OPLS3 molecular mechanics force field *via* the MacroModel (Ji and Xu, 2021) panel of Maestro 10.2. The conformers were then further optimized with the software package Gaussian 09 (Frisch et al., 2009) at the B3LYP/6-311G(2d, p) level, and the harmonic vibrational frequencies were also calculated to confirm their stability. Then the 60 lowest electronic transitions for the obtained conformers in vacuum were calculated using time-dependent density functional theory (TDDFT) methods at the B3LYP/6-311G(2d,p) level. ECD spectra of the conformers were simulated using a Gaussian function. The overall theoretical ECD spectra were obtained according to the Boltzmann weighting of each conformers.

α-glucosidase inhibition assay

The method used for the α-glucosidase inhibitory activity assay was based on previously reported literature (Fan et al., 2020). The reaction mixture consisted of 50 μL of PBS (100 mM, pH 7.0), 20 μL of *p*-NPG (25 mM) and 20 μL of the test compounds dissolved in DMSO at different concentrations. After incubation at 37°C for 10 min, 10 μL of the enzyme (2 U/mL) was added and the mixture was further incubated at 37°C for 30 min. Finally, the absorbance was measured at 405 nm on an automatic microplate reader. Acarbose was used as the positive control (IC_{50} = 12.2 ± 0.66 μM). All experiments were carried out in triplicate.

Enzyme kinetics of α-glucosidase inhibition assay

The Lineweaver–Burk plot was used to determine the inhibitory mode of **3** on α-glucosidase. The enzymatic reactions were performed and monitored with different concentrations of **3** (0, 100, 200, and 400 μM) and substrate (3.125, 6.25 and 12.5 mM), with the concentration of the enzyme being constant (0.5 U/mL). And the Dixon plot was used to calculated the inhibition constant (K_i) (He et al., 2021).

Molecular docking assay

The molecular docking simulations of **3** and **4** with α-glucosidase was performed according to the previously reported method (Chen et al., 2022). First, the chemical and MM2 energy minimized 3D structures of compounds **3** and **4** were obtained by using Chemdraw (20.0) and Chem3D (version 20.0), respectively. Meanwhile, the crystal structure of α-glucosidase (PDB ID: 3TOP) was obtained from the RCSB Protein Data Bank (www.rcsb.org). The AutoDock Vina was used to extract co-crystal ligands, determine the docking pocket and score the molecular docking of ligands and receptor protein. Finally, the visible results of possible binding sites were provided using PyMOL version 2.3.4.

Statistical analysis

The results were expressed as means ± standard deviations (n = 3). All of the data were analyzed by one-way analysis of variance (ANOVA) and following Tukey's test. GraphPad Prism 9.0 software was used for statistical analysis. A p value < 0.05 was considered statistically significant.

Results and discussion

Structure elucidation of the isolated compounds

Talarobenzofuran A (**1**) was isolated as yellow oil with the molecular formula of $C_{17}H_{22}O_7S$ deduced from HRESIMS at *m/z* 371.1168 $[M + H]^+$ (calcd for $C_{17}H_{23}O_7S$ 371.1159), corresponding to 7 degrees of unsaturation. The IR spectrum showed hydroxy and carbonyl absorption bands at 3420 cm^{-1}

and 1743 cm^{-1}, respectively. Analysis of the ^{1}H, ^{13}C and HSQC NMR data of **1** (Table 1 and Supplementary Figures S2–S4) displayed the presence of three methyls ($\delta_{C/H}$ 22.3/2.41, 26.2/1.20, 25.6/1.24), two methylenes ($\delta_{C/H}$ 34.6/3.37 and 3.52, 28.3/3.14 and 3.08), three methines ($\delta_{C/H}$ 91.8/4.69, 105.3/6.22, 70.6/4.43), one methoxy group ($\delta_{C/H}$ 52.6/3.73), three exchangeable protons (δ_H 9.79, 4.76, 3.70), six aromatic carbons (δ_C 112.5, 119.5, 139.7, 155.1, 164.9, 105.3), two carbonyl carbons (δ_C 173.6, 195.7) and one sp^3 hybrid carbon (δ_C 71.6), implying that two rings existed in **1** to match the 7 degrees of unsaturation. The ^{1}H and ^{13}C NMR data of **1** were similar with those of the co-isolated compound eurothiocin A (**4**) (Liu et al., 2014), indicating the presence of the benzofuran subunit. The HMBC correlations (Figure 2 and Supplementary Figure S6) from H-2 to C-7a (δ_C 164.9), from H_2-3 to C-3a, C-4 and C-7a, and from H-7 (δ_H 6.22) to C-3a, C-5 and C-7a, combined with the ^{1}H-^{1}H COSY correlations (Figure 2 and Supplementary Figure S5) of H-2/H_2-3 confirmed the presence of the benzofuran subunit. In addition, the HMBC correlations from the phenolic hydroxyl OH-4 (δ_H 9.79) to C-3a, C-4 and C-5, and from the aromatic methyl H_3-11 to C-5, C-6 and C-7 located the hydroxy and methyl group at C-4 and C-6, respectively. Furthermore, the HMBC correlations from H-2 to C-8, C-9, and C-10, from OH-8 to C-2, C-8, C-9 and C-10, and from the geminal methyl groups H_3-9 and H_3-10 to C-2 and C-8 indicated that the 2-hydroxypropan-2-yl group was located at C-2. Meanwhile, the ^{1}H-^{1}H COSY correlations of OH-14/H-14/H_2-13, together with the HMBC correlations from the methylene H_2-13 ($\delta_{C/H}$ 34.6/3.52 and 3.37) to the carbonyl carbons C-12 (δ_C 195.7) and C-15 (δ_C 173.6), from the oxymethine H-14 to C-15, from OH-14 to C-13, C-14 and C-15, and from H_3-16 to C-15 established the methyl lactate (C-13–C-16) moiety with the connection of C-13 and C-12 *via* the same sulfur atom to form thioester moiety. On the basis of the above results, the planar structure of **1** was elucidated as showed (Figure 1).

The relative configurations of C-2 and C-14 in **1** could not be assigned due to the lack of relevant ROESY correlations (Supplementary Figure S7). As the presence of a secondary alcohol at C-14, the modified Mosher's method (Ohtani et al., 1995) was performed to determine the absolute configuration of C-14. Treatment of **1** with (*S*)- or (*R*)-α-methoxy-α-trifluoromethylphenylacetyl chloride [(*S*)- or (*R*)-MTPA-Cl] in the presence of pyridine afforded the *R*-MTPA ester (**1a**) and *S*-MTPA ester (**1b**), respectively. The chemical shift differences ($\Delta\delta = \delta_{(S)\text{-MTPA-ester}} - \delta_{(R)\text{-MTPA-ester}}$) for the diastereomeric esters **1b** and **1a** were calculated in order to assign the absolute configuration at C-14. According to Mosher's rule, the absolute configuration at C-14 of **1** was clearly established as *S* (Figure 3).

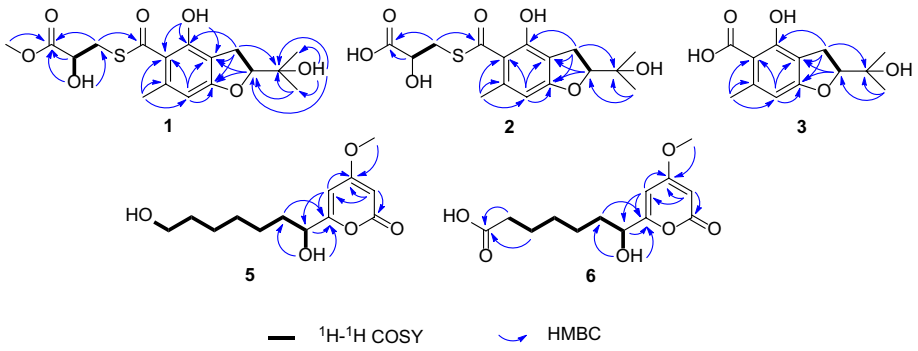

FIGURE 2
Key correlations of compounds 1–3 and 5–6.

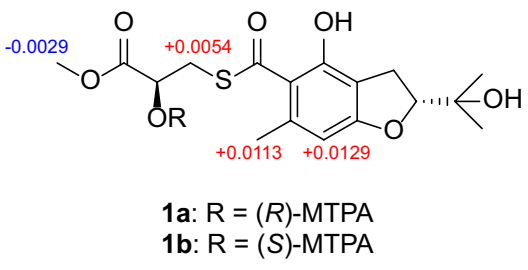

FIGURE 3
$\Delta\delta$ Values (in ppm) = $\delta_S - \delta_R$ obtained for (*S*)- and (*R*)-MTPA esters of 1b and 1a.

Then the absolute configuration of C-2 in **1** was deduced by a comparison of the experimental and calculated electronic circular dichroism (ECD) spectra generated by the time-dependent density functional theory (TDDFT) (Nugroho and Morita, 2014) for two stereoisomers (2*R*,14*S*)-**1** and (2*S*,14*S*)-**1** was performed. The experimental ECD curve of **1** matched well with the calculated ECD curve of (2*R*,14*S*)-**1** (Figure 4A), which allowed the elucidation of the absolute configuration of **1** as 2*R*,14*S*.

Talarobenzofuran B (**2**) was obtained as a yellow oil. Its molecular formula was determined as $C_{16}H_{20}O_7S$ (7 degrees of unsaturation) by HRESIMS (*m/z* 357.1010 $[M + H]^+$, calcd for $C_{16}H_{21}O_7S$ 357.1003), which is 14 mass units less than that of **1**. The NMR spectroscopic data (Table 1) of **2** were similar to those

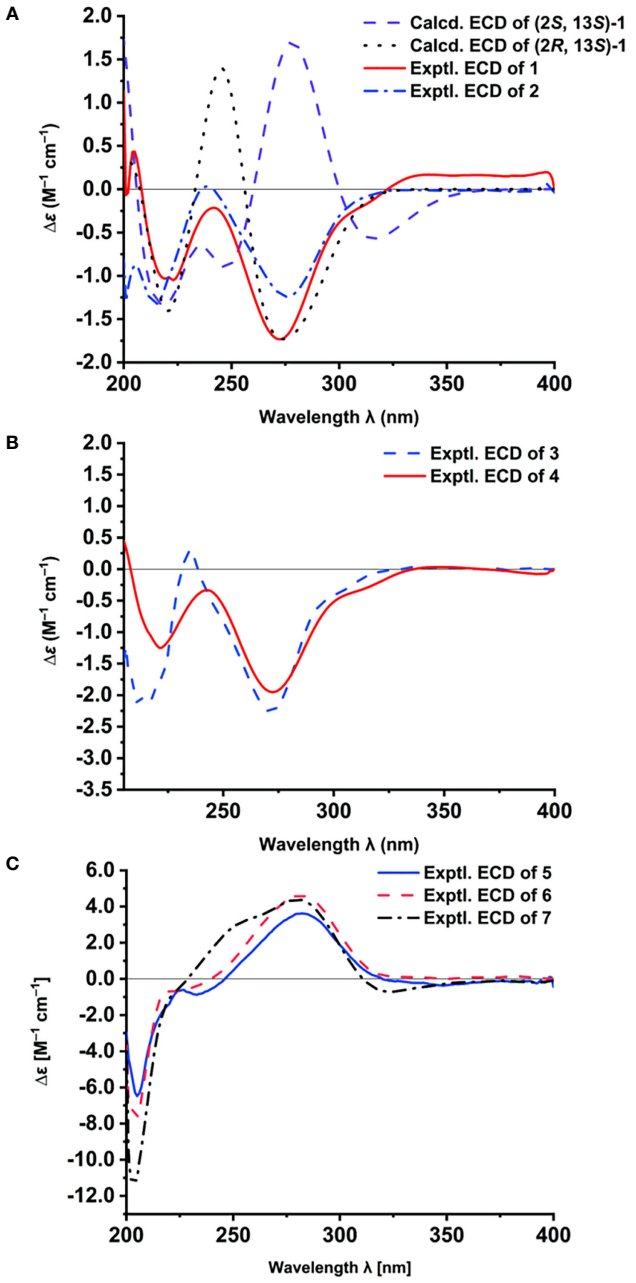

FIGURE 4
The ECD spectra of 1–7. Calculated and experimental ECD spectra of 1 and experimental ECD spectrum of 2 **(A)**; Experimental ECD spectra of 3 and 4 **(B)**; Experimental ECD spectra of 5–7 **(C)**.

of **1**, except that the methoxy group ($\delta_{C/H}$ 52.6/3.73) in **2** was replaced by a hydroxyl, which was supported by MS data and the HMBC correlations (Figure 2 and Supplementary Figure S12) from H_2-13 and H-14 to the carboxylic carbon C-15. The absolute configuration of **2** was deduced to be the same as that of **1** on the basis of biosynthetic consideration, which was further confirmed by the similar Cotton effects in the experimental ECD spectra of **1** and **2** (Figure 4A). Thus, the absolute configuration of compound **2** was designated as 2*R*,14*S*.

Talarobenzofuran C (**3**) was also obtained as a yellow oil. Its molecular formula was determined to be $C_{13}H_{16}O_5$ (6 degrees of unsaturation) by HRESIMS at *m/z* 253.1077 $[M + H]^+$ (calcd for $C_{13}H_{17}O_5$ 253.1071), which is 30 mass units less than that of eurothiocin A (**4**). Analyses of the 1D (Table 1 and Supplementary Figures S14, S15) and 2D (Figure 2 and Supplementary Figures S16-S18) NMR data of **3** indicated the same structure skeleton to that of **4**. The main difference was that the presence of the carboxylic group in **3** instead of the methyl thioester moiety, as evidenced by the MS data. On the basis of these results, the planar structure of **3** was elucidated (Figure 1). The experimental ECD spectrum of **3** (Figure 4B) showed similar Cotton effects with those of eurothiocin A (**4**) (Liu et al., 2014), indicating the *R* configuration at C-2. Therefore, the absolute configuration of compound **3** was established as 2*R*.

Talaropyrone A (**5**) was obtained as a light yellow solid with the molecular formula of $C_{13}H_{20}O_5$ deduced from the HRESIMS data (*m/z* 279.1206, $[M + Na]^+$, calcd for $C_{13}H_{20}O_5Na$ 279.1203), suggesting four degrees of unsaturation. Analysis of the ^1H, ^{13}C and HSQC NMR data of **5** (Table 2 and Supplementary Figures S19–S21) revealed the presence of two exchangeable protons (δ_H 5.59 and 4.32, respectively), one methoxy group ($\delta_{C/H}$ 56.3/3.81), six methylenes, one oxymethine ($\delta_{C/H}$ 68.9/4.23), four olefinic carbons with two protonated carbons and one carbonyl carbon (δ_C 163.3). Analysis of its 1D NMR data (Table 2 and Supplementary Figures S19, S20) revealed that the structure of compound **5** was closely related to that of compound **7** (Zhao et al., 2015), indicating the presence of the α-pyrone moiety. The noticeable difference was that the absence of NMR signals for a methyl and the presence of a methylene ($\delta_{C/H}$ 60.7/3.36) group and a hydroxyl (δ_H 4.23) group in **5**. The ^1H-^1H COSY (Figure 2 and Supplementary Figure S22) correlations of H_2-12/H_2-13, and the HMBC (Figure 2 and Supplementary Figure S23) correlations from OH-13 to C-12, from H_2-13 to C-11 showed that hydroxymethyl group was connected to C-12. The ECD spectrum (Figure 4C) and specific optical rotation of compound **5** were similar to those of nodulisporipyrone A (**7**) (Zhao et al., 2015), which indicated that the configuration of compound **5** was 7*R*. Thus, the structure of **5** was defined and named talaropyrone A.

Talaropyrone B (**6**) was obtained as white solid with the molecular formula $C_{13}H_{18}O_6$ based on HRESIMS data (*m/z* 293.1001, $[M + Na]^+$, calcd for $C_{13}H_{18}O_6Na$ 293.0996), which is 14 mass units more than that of **5**. The 1D NMR data (Table 2 and Supplementary Figures S24, S25) revealed that compound **6** had a similar core skeleton to compound **5**. The main difference was that the hydroxymethyl group at C-12 in compound **5** was replaced by a carboxyl group in compound **6**, which was further supported by HMBC correlations from H_2-11 and H_2-12 to the carbonyl carbon C-13 (δ_C 174.7) (Figure 2 and Supplementary Figure S28). The similar positive optical rotation and the similar ECD spectrum of **5** and **6** (Figure 4C) allowed the assignment of its absolute configuration 7*R* being the same as that of **5**. Thus, the structure of talaropyrone B (**6**) was established as shown.

On the basis of the NMR and MS spectroscopic data comparison with those optical reported in the literature, the structures of the known compounds were identified as eurothiocin A (**4**) (Liu et al., 2014), nodulisporipyrone A (**7**) (Zhao et al., 2015), peniazaphilin B (**8**) (Zhang et al., 2018), ramulosin (**9**) (Wang et al., 2014) and 6-hydroxyramulosin (**10**) (McMullin et al., 2017).

Structurally, compounds **1** and **2** possesed the unique thioester moiety derived from benzofuran and 2-hydroxy-3-mercaptopropionic acid, which was rarely-observed in natural products. Although several natural products with a methyl thioester group have been reported such as echinomycin (Watanabe et al., 2006), thiocoraline (Al-Mestarihi et al., 2014), lincomycin A (Spížek and Řezanka, 2017) and collismycin A (Garcia et al., 2012), compounds **1** and **2** possesed previously undescribed lactyl thioester moiety. Compound **3** is a new analogue of the benzofuran **4**. While compounds **5** and **6** are new α-pyrone derivatives. Biogenetically, the aromatic polyketide orsellinic acid, which was biosynthesized from one unit of acetyl-CoA and three units of malonyl-CoA (Hashimoto et al., 2014), could be the biosynthetic precursor for compounds **1**–**4**, first *via* isoprenylation, oxidation and dehydration reactions to form compound **3**. Subsequently, compound **3** undergoes a thioesterification reaction to generate compound **4**. In addition, compound **3** combines with cysteine *via* thioesterification, deamination and methylation reactions to form **1** and **2**. The proposed biosynthetic pathways of compounds **1**–**4** was illustrated in Scheme 1.

Biological activity

Compounds **1**–**10** were also evaluated for antibacterial activities against *Staphylococcus aureus* (CGMCC 1.2465), *Streptococcus pneumoniae* (CGMCC 1.1692), *Escherichia coli* (CGMCC 1.2340) and *Bacillus subtilis* (ATCC 6633), and none of these compounds showed antibacterial activities toward these bacteria (MIC > 50 μg/mL). Meanwhile, compounds **1**–**10** were evaluated for the *in vitro* α-glucosidase inhibitory activities (Table 3). Compounds **3** and **4** showed moderate inhibitory effect with IC_{50} values of 48.9 ± 2.16 and 8.8 ± 1.08 μM,

10.3389/fmars.2022.1034945

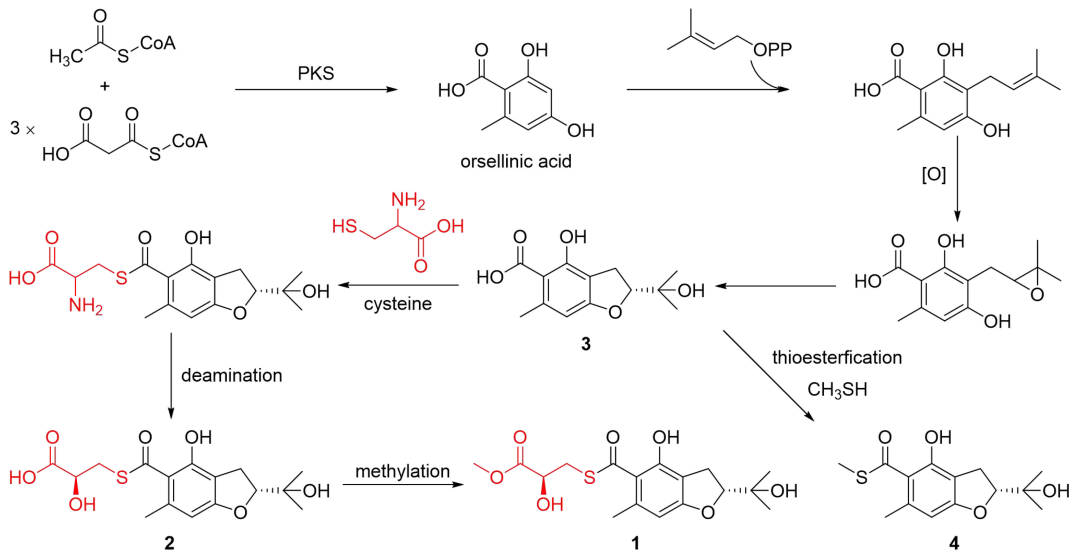

SCHEME 1
Proposed biosynthetic pathways of compounds **1**–**4**.

TABLE 3 α-glucosidase inhibitory activities.

Compounds	IC_{50} (μM)	Compounds	IC_{50} (μM)
1	>100	**6**	>100
2	>100	**7**	>100
3	48.9 ± 2.16	**8**	>100
4	8.8 ± 1.08	**9**	>100
5	>100	**10**	>100
Acarbose	12.2 ± 0.66		

respectively (acarbose as positive control with IC_{50} value of 12.2 ± 0.66 μM).

To gain some insight about the inhibitory type of **3** on α-glucosidase, Lineweaver–Burk double reciprocal and Dixon single reciprocal plots were used to analyzed the data and determined the inhibit mode. In the Lineweaver–Burk plot, the *Vmax* value decreased with the increment of concentration, and the lines intersected on the *x*-axis (*p*-NPG concentrations), suggesting that the K_m value was unchanged, implying the non-competitive-type inhibition of **3** (Figure 5A). Dixon plot was drawn by plotting the reciprocal of velocity against inhibitory concentrations at varying concentrations of *p*-NPG and the K_i value of **3** was further calculated as 242.3 μM (Figure 5B).

The molecular docking study was performed to identify the possible orientations and binding interactions of the **3** and **4** in the active site of the α-glucosidase. The molecular docking models of **3** and **4** are illustrated in Figure 6. The results of docking revealed that **3** formed two hydrogen bonds with Arg-1510 and Asp-1526 residues (Figure 6A), **4** formed two hydrogen bonds with Arg-1510 and His-1584 residues (Figure 6B). The different hydrogen bonding sites may result in different inhibitory effects, and the results of this docking experiment may help to understanding the binding mechanism of benzofurans and α-glucosidase.

Conclusion

In summary, five new compounds including two thionic benzofurans talarobenzofurans A and B (**1** and **2**), one benzofuran talarobenzofuran C (**3**) and two α-pyrones talaropyrones A and B (**5** and **6**), along with five known ones were isolated from the fermentation of the mangrove-derived fungus *Talaromyces* sp. WHUF0341 guided by OSMAC strategy. Compounds **1** and **2** possesed the unique thioester moiety derived from benzofuran and 2-hydroxy-3-mercaptopropionic acid. Compounds **3** and **4** exhibited inhibitory effects against α-

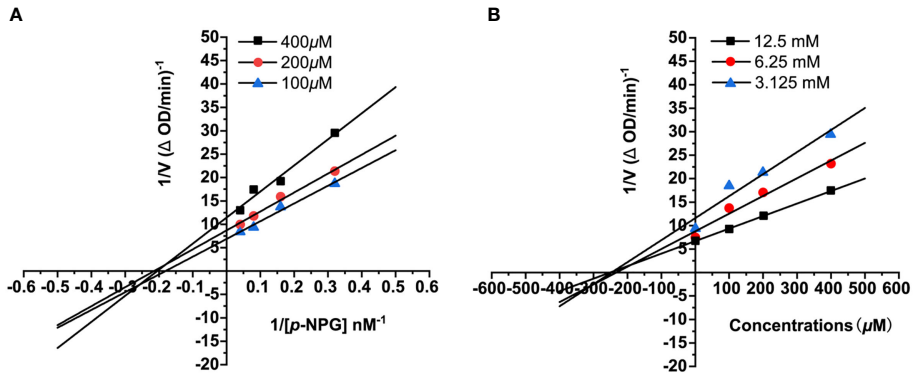

FIGURE 5
The Lineweaver–Burk **(A)** and Dixon **(B)** plots for α-glucosidase inhibition of compound 3.

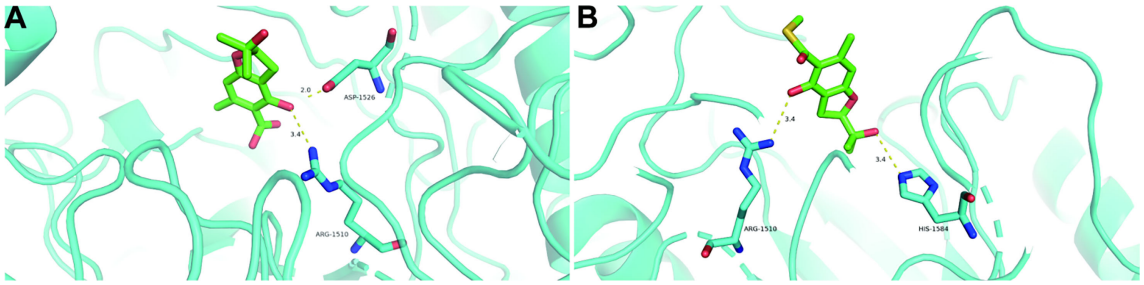

FIGURE 6
Docking poses and interactions of 3 **(A)** and 4 **(B)** with α-glucosidase (PDB ID: 3TOP). Hydrogen bond was denoted with yellow dash line.

glucosidase activity. The enzyme kinetics assay indicated the non-competitive-type inhibition of **3** towards α-glucosidase. Furthermore, the interactions of **3** and **4** with α-glucosidase were investigated by molecular docking assay. And the biosynthetic pathways of compounds **1**–**4** was also proposed. These findings not only expanded the chemical diversities of the natural benzofuran and α-pyrone families, but also provided valuable clues for searching new antidiabetic candidates from the mangrove-derived fungi.

Data availability statement

The datasets presented in this study can be found in online repositories. The names of the repository/repositories and accession number(s) can be found in the article/Supplementary Material.

Author contributions

Conceptualization: LL. Methodology: RZ, JZ and RH. Resources: RZ, YX and KH. Data curation, RZ, JZ, and RH. Writing–original draft preparation: RZ and JZ. Writing–review and editing: RH, KH, and LL. Project administration and funding acquisition: LL. All authors contributed to the article and approved the submitted version.

Funding

This research was funded by grants from National Key Research and Development Program of China (2021YFC2100600 and 2018YFC0311000) and the National Natural Science Foundation of China (32022002 and 21977113).

Acknowledgments

The authors thank the National Special Project and the National Natural Science Foundation for funding. We also appreciate Junnan Shen and Desheng Li (School of Pharmaceutical Sciences, Wuhan University) for their contribution on strain isolation.

Conflict of interest

The authors declare that the research was conducted in the absence of any commercial or financial relationships that could be construed as a potential conflict of interest.

Publisher's note

All claims expressed in this article are solely those of the authors and do not necessarily represent those of their affiliated organizations, or those of the publisher, the editors and the reviewers. Any product that may be evaluated in this article, or claim that may be made by its manufacturer, is not guaranteed or endorsed by the publisher.

Supplementary material

The Supplementary Material for this article can be found online at: https://www.frontiersin.org/articles/10.3389/fmars.2022.1034945/full#supplementary-material

References

Al-Mestarihi, A. H., Villamizar, G., Fernández, J., Zolova, O. E., Lombó, F., and Garneau-Tsodikova, S. (2014). Adenylation and *S*-methylation of cysteine by the bifunctional enzyme TioN in thiocoraline biosynthesis. *J. Am. Chem. Soc* 136, 17350–17354. doi: 10.1021/ja510489j

Carroll, A. R., Copp, B. R., Davis, R. A., Keyzers, R. A., and Prinsep, M. R. (2021). Marine natural products. *Nat. Prod. Rep.* 38, 362–413. doi: 10.1039/D0NP00089B

Chen, S. J., Tian, D. M., Wei, J. H., Li, C., Ma, Y. H., Gou, X. S., et al. (2022). Citrinin derivatives from *Penicillium citrinum* Y34 that inhibit α-glucosidase and ATP-citrate lyase. *Front. Mar. Sci.* 9. doi: 10.3389/fmars.2022.961356

El-Bondkly, E. A. M., El-Bondkly, A. A. M., and El-Bondkly, A. A. M. (2021). Marine endophytic fungal metabolites: A whole new world of pharmaceutical therapy exploration. *Heliyon* 7, e06362. doi: 10.1016/j.heliyon.2021.e06362

Ellison, A. M., and Farnsworth, E. J. (1992). The ecology of belizean mangrove-root fouling communities: Patterns of epibiont distribution and abundance, and effects on root growth. *Hydrobiologia* 247, 87–98. doi: 10.1016/0022-0981(90)90139-4

Fan, J. R., Kuang, Y., Dong, Z. Y., Yi, Y., Zhou, Y. X., Li, B., et al. (2020). Prenylated phenolic compounds from the aerial parts of *Glycyrrhiza uralensis* as PTP1B and α-glucosidase inhibitors. *J. Nat. Prod.* 83, 814–824. doi: 10.1021/acs.jnatprod.9b00262

Frisch, M. J., Trucks, G. W., Schlegel, H. B. M., Scuseria, G. E., Robb, M. A., Cheeseman, J. R., et al. (2009). Gaussian 09, revision A.1.

Garcia, I., Vior, N. M., Brana, A. F., Gonzalez-Sabin, J., Rohr, J., Moris, F., et al. (2012). Elucidating the biosynthetic pathway for the polyketide-nonribosomal peptide collismycin a: Mechanism for formation of the 2,2'-bipyridyl ring. *Chem. Biol.* 19, 399–413. doi: 10.1016/j.chembiol.2012.01.014

Guo, W. Q., Kong, X. L., Zhu, T. J., Gu, Q. Q., and Li, D. H. (2015). Penipyrols A–B and peniamidones A–D from the mangrove derived *Penicillium solitum* GWQ-143. *Arch. Pharm. Res.* 38, 1449–1454. doi: 10.1007/s12272-014-0513-3

Hashimoto, M., Nonaka, T., and Fujii, I. (2014). Fungal type III polyketide synthases. *Nat. Prod. Rep.* 31, 1306–1317. doi: 10.1039/C4NP00096J

He, X. F., Chen, J. J., Huang, X. Y., Hu, J., Zhang, X. K., Guo, Y. Q., et al. (2021). The antidiabetic potency of *Amomum tsao-ko* and its active flavanols, as PTP1B selective and α-glucosidase dual inhibitors. *Ind. Crop Prod.* 160, 112908. doi: 10.1016/j.indcrop.2020.112908

Hemberger, Y., Xu, J., Wray, V., Proksch, P., Wu, J., and Bringmann, G. (2013). Pestalotiopens A and B: stereochemically challenging flexible sesquiterpene-cyclopaldic acid hybrids from *Pestalotiopsis* sp. *Chem. Eur. J.* 19, 15556–15564. doi: 10.1002/chem.201302204

Hou, B. L., Liu, S. S., Huo, R. Y., Li, Y. Q., Ren, J. W., Wang, W. Z., et al. (2021). New diterpenoids and isocoumarin derivatives from the mangrove-derived fungus *Hypoxylon* sp. *Mar. Drugs* 19, 362. doi: 10.3390/md19070362

Ji, C. F., and Xu, X. Z. (2021). Recent advancements of macrolide hybrids against *Staphylococcus aureus*. *Curr. Top. Med. Chem.* 21, 2455–2473. doi: 10.2174/1568026620999201203213733

Liu, H. B., Liu, Z. M., Chen, Y. C., Tan, H. B., Li, S. N., Li, D., et al. (2021a). Cytotoxic diaporindene and tenellone derivatives from the fungus *Phomopsis lithocarpus*. *Chin. J. Nat. Med.* 19, 874–880. doi: 10.1016/s1875-5364(21)60095-x

Liu, G. R., Niu, S. B., and Liu, L. (2021b). Alterchromanone A, one new chromanone derivative from the mangrove endophytic fungus *Alternaria longipes*. *J. Antibiot. (Tokyo).* 74, 152–155. doi: 10.1038/s41429-020-00364-4

Liu, S., Su, M. Z., Song, S. J., Hong, J. K., Chung, H. Y., and Jung, J. H. (2018). An anti-inflammatory PPAR-γ agonist from the jellyfish-derived fungus *Penicillium chrysogenum* J08NF-4. *J. Nat. Prod.* 81, 356–363. doi: 10.1021/acs.jnatprod.7b00846

Liu, Z. M., Xia, G. P., Chen, S. H., Liu, Y. Y., Li, H. X., and She, Z. G. (2014). Eurothiocin A and B, sulfur-containing benzofurans from a soft coral-derived fungus *Eurotium rubrum* SH-823. *Mar. Drugs* 12, 3669–3680. doi: 10.3390/md12063669

McMullin, D. R., Green, B. D., Prince, N. C., Tanney, J. B., and Miller, J. D. (2017). Natural products of *Picea* endophytes from the Acadian forest. *J. Nat. Prod.* 80, 1475–1483. doi: 10.1021/acs.jnatprod.6b01157

Meng, L. H., Wang, C. Y., Mándi, A., Li, X. M., Hu, X. Y., Kassack, M. U., et al. (2016). Three diketopiperazine alkaloids with spirocyclic skeletons and one bisthiodiketopiperazine derivative from the mangrove-derived endophytic fungus *Penicillium brocae* MA-231. *Org. Lett.* 18, 5304–5307. doi: 10.1021/np400614f

Nagelkerken, I., Blaber, S. J. M., Bouillon, S., Green, P., Haywood, M., Kirton, L. G., et al. (2008). The habitat function of mangroves for terrestrial and marine fauna: a review. *Aquat. Bot.* 89, 155–185. doi: 10.1016/j.aquabot.2007.12.007

Newman, D. J., and Cragg, G. M. (2020). Natural products as sources of new drugs over the nearly four decades from 01/1981 to 09/2019. *J. Nat. Prod.* 83, 770–803. doi: 10.1021/acs.jnatprod.9b01285

Nugroho, A. E., and Morita, H. (2014). Circular dichroism calculation for natural products. *J. Nat. Med.* 68, 1–10. doi: 10.1007/s11418-013-0768-x

Ohtani, I. I., Hotta, K., Ichikawa, Y., and Isobe, M. (1995). Application of modified mosher's method to α-aromatic secondary alcohols. exception of the rule and conformational analyses. *Chem. Lett.* 24, 513–514. doi: 10.1246/cl.1995.513

Pan, R., Bai, X. L., Chen, J. W., Zhang, H. W., and Wang, H. (2019). Exploring structural diversity of microbe secondary metabolites using OSMAC strategy: a literature review. *Front. Microbiol.* 10. doi: 10.3389/fmicb.2019.00294

Spížek, J., and Řezanka, T. (2017). Lincosamides: chemical structure, biosynthesis, mechanism of action, resistance, and applications. *Biochem. Pharmacol.* 133, 20–28. doi: 10.1016/j.bcp.2016.12.001

Tao, L. Y., Zhang, J. Y., Liang, Y. J., Chen, L. M., Zhen, L. S., Wang, F., et al. (2021). Cytotoxic diaporindene and tenellone derivatives from the fungus *Phomopsis lithocarpus*. *Chin. J. Nat. Med.* 19, 874–880. doi: 10.3390/md8041094

Valente, S., Cometto, A., Piombo, E., Meloni, G. R., Ballester, A. R., González-Candelas, L., et al. (2020). Elaborated regulation of griseofulvin biosynthesis in *Penicillium griseofulvum* and its role on conidiation and virulence. *Int. J. Food Microbiol.* 328, 108687. doi: 10.1016/j.ijfoodmicro.2020.108687

Wang, J. Y., Wang, G. P., Zhang, Y. L., Zheng, B. Q., Zhang, C. L., and Wang, L. W. (2014). Isolation and identification of an endophytic fungus *Pezicula* sp. in *Forsythia viridissima* and its secondary metabolites. *World. J. Microbiol. Biotechnol.* 30, 2639–2644. doi: 10.1007/s11274-014-1686-0

Watanabe, K., Hotta, K., Praseuth, A. P., Koketsu, K., Migita, A., Boddy, C. N., et al. (2006). Total biosynthesis of antitumor nonribosomal peptides in *Escherichia coli*. *Nat. Chem. Biol.* 2, 423–428. doi: 10.1038/nchembio803

Yu, G. H., Zhou, G. L., Zhu, M. L., Wang, W., Zhu, T. J., Gu, Q. Q., et al. (2016). Neosartoryadins A and B, fumiquinazoline alkaloids from a mangrove-derived fungus *Neosartorya udagawae* HDN13-313. *Org. Lett.* 18, 244–247. doi: 10.1021/acs.orglett.5b02964

Zhang, D. W., Zhao, J. Y., Wang, X. W., Zhao, L. L., Liu, H. Y., Wei, Y. Z., et al. (2018). Peniazaphilin A, a new azaphilone derivative produced by *Penicillium* sp. CPCC 400786. *J. Antibiot.* 71, 905–907. doi: 10.1038/s41429-018-0077-4

Zhao, Q., Wang, C. X., Yu, Y., Wang, G. Q., Zheng, Q. C., Chen, G. D., et al. (2015). Nodulisporipyrones A–D, new bioactive α-pyrone derivatives from *Nodulisporium* sp. *J. Asian Nat. Prod. Res.* 17, 567–575. doi: 10.1080/10286020.2015.1040776